Catalysis Communications 148 (2021) 106181

Contents lists available at ScienceDirect

Catalysis Communications

journal homepage: www.elsevier.com/locate/catcom

Short communication

3D-printing of metallic honeycomb monoliths as a doorway to a new generation of catalytic devices: the Ni-based catalysts in methane dry reforming showcase

Fazia Agueniou[a], Hilario Vidal[a,*], Juan de Dios López[a], Juan C. Hernández-Garrido[a], Miguel A. Cauqui[a], Francisco J. Botana[a], José J. Calvino[a], Vladimir V. Galvita[b], José M. Gatica[a]

[a] Departamento de Ciencia de los Materiales e Ingeniería Metalúrgica y Química Inorgánica, e IMEYMAT, Instituto Universitario de Investigación en Microscopía Electrónica y Materiales, Universidad de Cádiz, 11510 Puerto Real, Spain
[b] Ghent University, Laboratory for Chemical Technology, Technologiepark 914, B-9052 Gent, Belgium.

ARTICLE INFO

Keywords:
3D-printing
Stainless-steel honeycomb
Nickel
Ceria-Zirconia
Dry reforming of methane

ABSTRACT

Stainless-steel honeycomb monoliths (square cell-shape/230 cpsi cylinders) were 3D-printed and used as support of a Ni/CeO_2-ZrO_2 powder deposited by washcoating. The resulting catalysts were characterized by XRF, SEM-EDX and H_2-TPR, and tested in the dry reforming of methane reaction. In the 750–900 °C range, they showed competitive conversions (45–95%) and H_2/CO ratio (0.84–0.94) compared to cordierite honeycombs with same catalyst loading and geometric characteristics, but did not require activation time thanks to better heat transfer. Both structured catalysts were stable in prolonged TOS experiments. The bare metallic monoliths exhibited significant activity at 900 °C due to their intrinsic nickel content.

1. Introduction

Metallic honeycomb monoliths are used in heterogeneous catalysis due to their intrinsic advantage regarding heat transfer facilitation among other properties with respect to their ceramic counterparts [1,2]. On the contrary, they exhibit the drawback of a poorer adherence to washcoated catalysts [3]. Conventionally prepared by the corrugation method [2,4], such limitation is overcome by subsequent chemical-thermal treatments that provide surface roughness on the metal sheets to which the deposited phase may anchor [2,5–7].

Lately, the development of 3D-printing techniques has opened up a fascinating window to the manufacture of a quasi-unlimited variety of structured materials with projection in many fields of science, including catalysis [8]. The potential of these procedures is highly attributed to the possibility of controlling both geometry and rugosity of the final device due to the inherent building principles. The former might be crucial in the case of a structured reactor to optimize the heat and mass transfer within its channels, while the latter could ideally avoid the time and energy consuming steps. Additionally, we cannot discard the chance of selecting appropriate raw materials which might include the metal desired as active phase in the final catalyst, thus excluding the need of further incorporation. The still scarce literature related to the catalytic applications of 3D-printed structured reactors is mainly focused on plastic and ceramic substrates [9–11], being those based on a metallic matrix but reduced to a few examples dealing with foam-like products rather than honeycomb monoliths [12,13].

Recently, we showed that it is possible to obtain honeycomb monolithic catalysts with outstanding activity and stability in the dry reforming of methane (DRM) by washcoating commercial cordierites with Ni-based catalysts, even employing ultrathin washcoat of very low loading [14]. Therefore, it would be interesting to investigate a similar approach with metallic honeycombs as support. Certainly, numerous studies were already reported in which metallic monoliths were used in related catalytic processes [15–17], especially in methane steam reforming [18–21], but none of them specifically focused on DRM. Moreover, the work presented here proposes for the first time to the best of our knowledge the 3D-printing of metallic monoliths which replicates real honeycomb design (i.e. structures with multiple straight parallel channels in the flow direction) and their application to a heterogeneous catalytic process. In this preliminary stage of research, we have intentionally limited the manufacture to honeycomb monoliths with the same geometry and cell density of the previously tested cordierite counterparts [14] for ease of comparison. Indeed, DRM was selected not so much as a goal but as a tool to evaluate and compare with previous references the potential of the fabricated devices and the worthiness of their further optimization and/or extrapolation to other

* Corresponding author.
E-mail address: hilario.vidal@uca.es (H. Vidal).

https://doi.org/10.1016/j.catcom.2020.106181
Received 10 July 2020; Received in revised form 2 October 2020; Accepted 3 October 2020
Available online 06 October 2020
1566-7367/

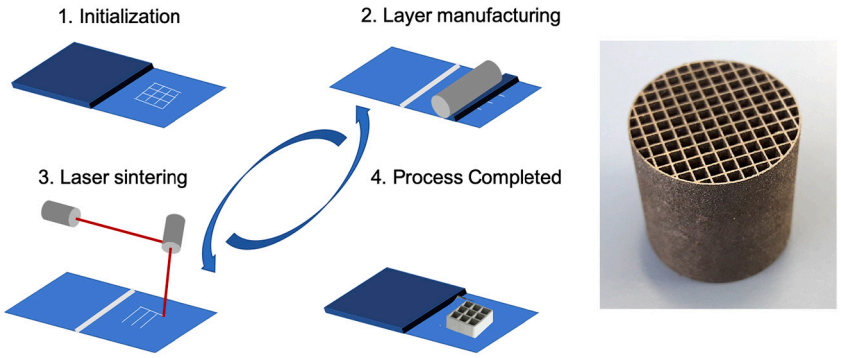

Fig. 1. Schematic representation of the followed 3D printing procedure by Selective Laser Sintering and image of a final 3D-printed metallic honeycomb monolith. 1) Initialization of the printing procedure with the preparation of the metallic powder and the computer aided design (CAD) for the object to be printed; 2) Dispersion of thin layer of powder over the platform; 3) Selective melting by the laser; and after several cycles for steps 2 & 3; 4) Final 3D-printed object. Further calcination in N_2 at 525 °C for 4 h was applied to eliminate strains caused by 3D printing.

Table 1
Geometric characteristics of the 3D-printed metallic honeycomb monoliths.

Cell shape	Square
Cell density (cpsi; cells/cm^2)	230; 35.7
Cell spacing (mm)	1.7
Wall thickness (mm)	0.27
Dh (mm)	1.2
GSA (cm^2/cm^3)	20.2
OFA (%)	61
Height (cm)	2.5
External diameter (cm)	2.0
Weight (g)	10.64

processes of exothermic character.

2. Experimental

2.1. Catalyst preparation

The raw material for the 3D manufacturing of the metallic honeycomb monoliths was a commercial stainless-steel (AISI 15-5PH) powder (particle size below 63 μm) provided by EOS with the following minority elements content (max. wt%): Cr, 14–15.5; Ni, 3.5–5.5; Cu, 2.5–4.5; Mn, 1; Si, 1; C, 0.07; Mo, 0.5; Nb, 0.45. The 3D printing was performed through Direct Metal Laser Sintering (DMLS) [22] using a DMLS EOS M290 machine. It had a 400 W Yb laser fibre controlled by F-theta lens and producing a beam diameter of 100 μm. A nitrogen generator inside the system was used to avoid the oxidation of the parts. The honeycomb monoliths were built along the vertical direction with a layer thickness of 40 μm, using a building platform pre-heated at 100 °C in nitrogen atmosphere (Fig. 1).

A powdered ceria-zirconia supported nickel catalyst (4.5 wt% of Ni content and Ce/Zr mixed oxide with 18/82 molar ratio) prepared as previously reported [14], was selected as the catalytic phase to be deposited onto the 3D-printed honeycombs. Such deposition was performed by a washcoating procedure from a slurry (stabilized at pH 4.0 using acetic acid) containing the nickel-based catalyst, following the methodology well described previously [23]. Briefly, the prepared slurries contained the catalyst powder (19.1 wt%), polyvinyl alcohol (1.7 wt%), Nyacol AL20 colloidal alumina (4.2 wt%) and water. The 3D-printed metallic monolith pieces (Table 1) were immersed (3 cm min^{-1}) in this slurry, kept fully immersed for 90 s, with the first 15 s under ultra-sonication. They were then pulled out at the same rate, and the excess of slurry was removed by air flowing. The pieces were then dried at 120 °C for 30 min, and finally calcined (5 °C min^{-1}) at 450 °C (1 h). The reached active phase loading was estimated from the weight gain after calcination. The coating adherence was evaluated from the weight loss after immersion of the monoliths in petroleum ether under ultrasounds (30 min).

2.2. Catalysts characterization

The prepared catalysts were characterized by X-ray micro-fluorescence (XRF) in a Bruker S4 Pioneer spectrophotometer. They were also studied by scanning electron microscopy (SEM), obtaining (unless indicated) both images and Energy-dispersive X-ray (EDX) compositional analysis spectra in a FEG Nova NanoSEM 450 microscope operating at 30 kV. Additionally, H_2 Temperature-Programmed Reduction (H_2-TPR) profiles were recorded in an Autochem II 2920 equipped with thermal conductivity detector (TCD).

2.3. Catalytic tests

The catalytic performance of the various monoliths (bare and washcoated) in the DRM reaction was evaluated in quartz reactors at atmospheric pressure and in the 750–900 °C range, using a 1:1 gas mixture of CH_4 and CO_2 as feedstock and a WHSV of 115 L g^{-1} h^{-1}. In all cases, a pre-treatment of the monolith with 60 mL min^{-1} H_2(5%)/Ar at 600 °C (2 h) was applied. The gas analysis at the inlet and outlet of the reactor was performed by gas chromatography (Bruker 450-GC). Reactants (CH_4 and CO_2) conversion values were estimated from the inlet and outlet molar fractions of the individual gases according to the following Eqs. (1)–(2):

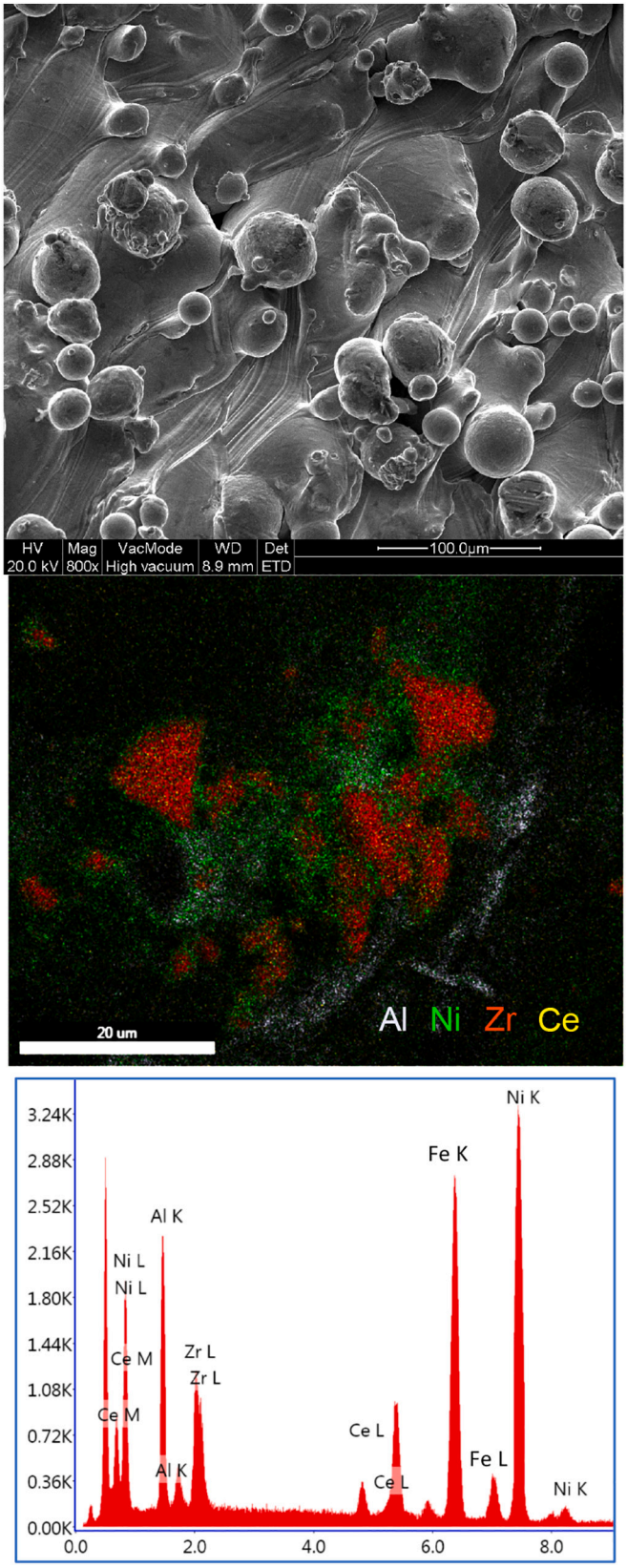

Fig. 2. SEM image corresponding to a piece of the bare metallic monolith acquired in a FEG-SEM microscope (FEI Quanta 200 + EDAX), and EDX compositional mapping of a piece of the washcoated monolith with its corresponding EDX spectrum.

$$CH_4\ \text{Conversion}\ (\%) = 100 \times \frac{[CH_4]_{inlet} - [CH_4]_{outlet}}{[CH_4]_{inlet}} \quad (1)$$

$$CO_2\ \text{Conversion}\ (\%) = 100 \times \frac{[CO_2]_{inlet} - [CO_2]_{outlet}}{[CO_2]_{inlet}} \quad (2)$$

The molar fractions at the outlet of the reactor were corrected to account for the volumetric change due to the DRM reaction.

A complementary study was done through Temperature-Programmed (TP) Reaction experiments, heating (5 °C min^{-1}) the samples under a flow of CH_4(20%)/CO_2(20%)/He and using mass spectrometer (Pfeiffer QSM-200) as gas analyzer.

3. Results and discussion

3.1. Characterization of the monolithic catalysts

The average specific loading of the washcoated metallic monoliths resulted to be 0.39 mg/cm^2. This value is very similar to that previously found for the same preparation employing cordierite monoliths as support [14]. This is a first signal that the 3D-printing procedure led to a metal substrate having adequate surface roughness. In fact, the adherence of the washcoat was 68%, a value that although apparently low, it is much higher than that of corrugated monoliths without any further surface treatment, in which it is almost zero [24]. It is also in the order of the adherence of alumina washcoats deposited on metallic supports pre-oxidized between 800 and 1050 °C for even 10 h [25,26], and also similar or slightly lower than that reported for some zinc [5] and manganese [6] oxides-washcoated FeCralloy monoliths in which the substrate was previously obtained by corrugation followed by heating in air at 900 °C for 22 h.

The use of SEM confirmed the 3D-printed monolith roughness (Fig. 2 and Fig. S1 in Supplementary Electronic Information, ESI). Moreover, coupled EDX compositional analysis at the micron scale allowed detecting the phase deposited over the metallic monolith walls; the mapping performed in a wall region of the washcoated monolith in which the presence of Ni, Ce and Zr is clearly observed. The quantitative analysis by means of the corresponding EDX spectrum indicated a higher Ni content than that expected for the catalyst formulation, which is attributed to the contribution of Ni originally present in the stainless-steel used to print the honeycomb. This result is consistent with the X-ray micro-fluorescence analysis carried out over a similar reduced area of the surface (Fig. 3), which also evidenced a partial coating of the monolith walls by the active phase. Moreover, both techniques (XRF and SEM-EDX) suggest an appropriate Ni-Ce-Zr interaction in the zones where the deposits of catalyst are found, since the signals of the three elements are present at the same or nearby locations. This scenario also resembles that previously observed after washcoating cordierites with the same nickel powdered catalyst [14].

Fig. 4 shows the result of the H_2-TPR experiment over the washcoated monolithic catalyst. The curve derived from the bare monolith is included as a reference. In general, the detailed interpretation of H_2-TPR profiles of nickel supported on ceria-zirconia binary oxides is difficult [27] because the temperature for the supported NiO reduction may change as function of different distribution of particle sizes and/or degrees of interaction with the support [28,29]. Moreover, reduction of the support and nickel species can occur simultaneously, promoted by the spillover of hydrogen species [30,31], thus significantly lowering the temperature at which the ceria-zirconia mixed oxide is reduced.

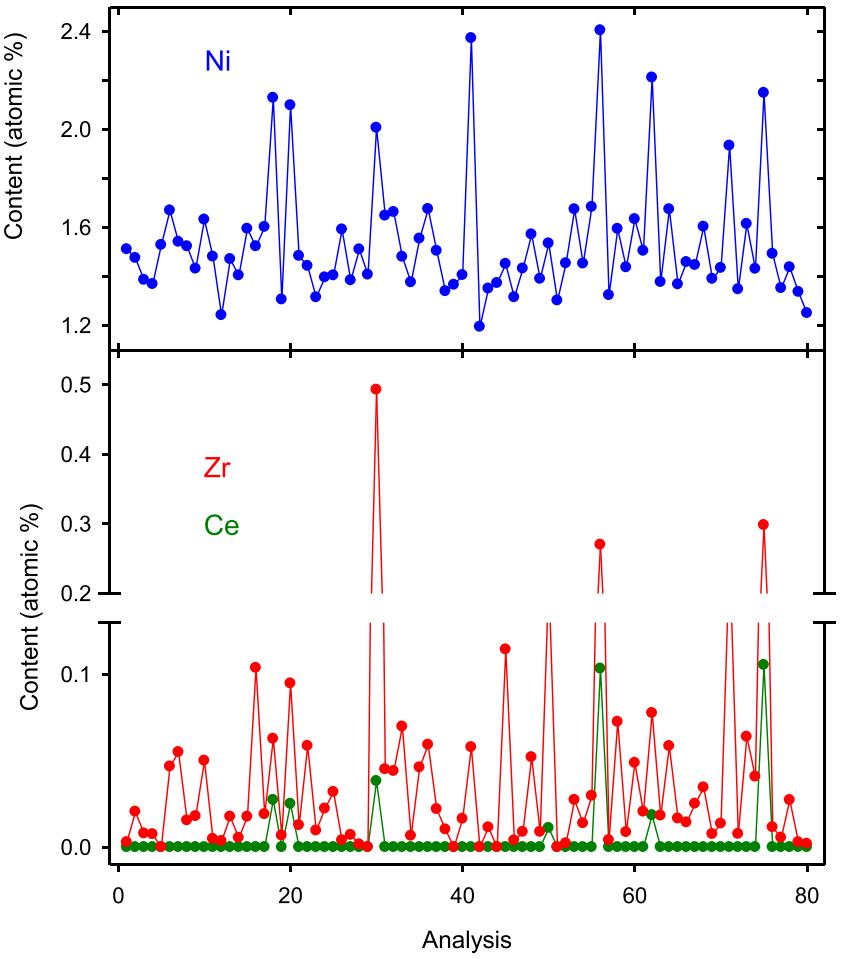

Fig. 3. Micro-XRF analysis representative of the walls surface of the washcoated metallic monolith.

Nevertheless, considering our previous experience with the same catalyst supported onto cordierite monoliths [14], we can reasonably assign the reduction peak that dominates the signal, centered around 370 °C, to the reduction of nickel species. It should be noted that in the H_2-TPR curve of the bare monolith, almost negligible reduction is comparatively observed, as expected for a stainless steel.

The results presented and discussed above allowed to select 600 °C as the catalyst activation temperature, as far as this temperature guaranties that the entire nickel and most of the cerium contained in the washcoated monolith are in a reduced form, a prerequisite well-stablished for obtaining better catalytic results in the DRM reaction [32].

3.2. Catalytic performance evaluation

Aiming to establish the operating conditions in the DRM reaction for the present catalyst, semi-quantitative TP reaction profiles of the evolution of CO_2, CH_4, CO, H_2 and H_2O by means of mass spectrometry were recorded (Fig. S2, ESI). Remarkable, the reaction abruptly activated ~600 °C, temperature at which CH_4 and CO_2 consumption along with CO and H_2 production were detected. As it is well-known, the DRM process may occur simultaneously with several secondary reactions [33]. In fact, H_2O formation was detected throughout the whole temperature range, where catalytic activity was observed, indicating that the Reverse Water Gas Shift (RWGS) reaction occurs in parallel with DRM. Furthermore, CO_2 conversion values were always higher than those of CH_4, and the H_2/CO ratios in the outlet gas were lower than 1.

Fig. 5 summarizes the main results obtained in the DRM reaction at three different temperatures (750, 800 and 900 °C). They first illustrate the competitiveness of the washcoated metallic monolith compared to the same washcoated Ni-based catalyst on cordierite previously reported [14]. Although the latter showed better conversions and H_2/CO ratio at 750 °C, the differences between the two structured catalysts decreased at 800 °C, and observing a reversal of the relative

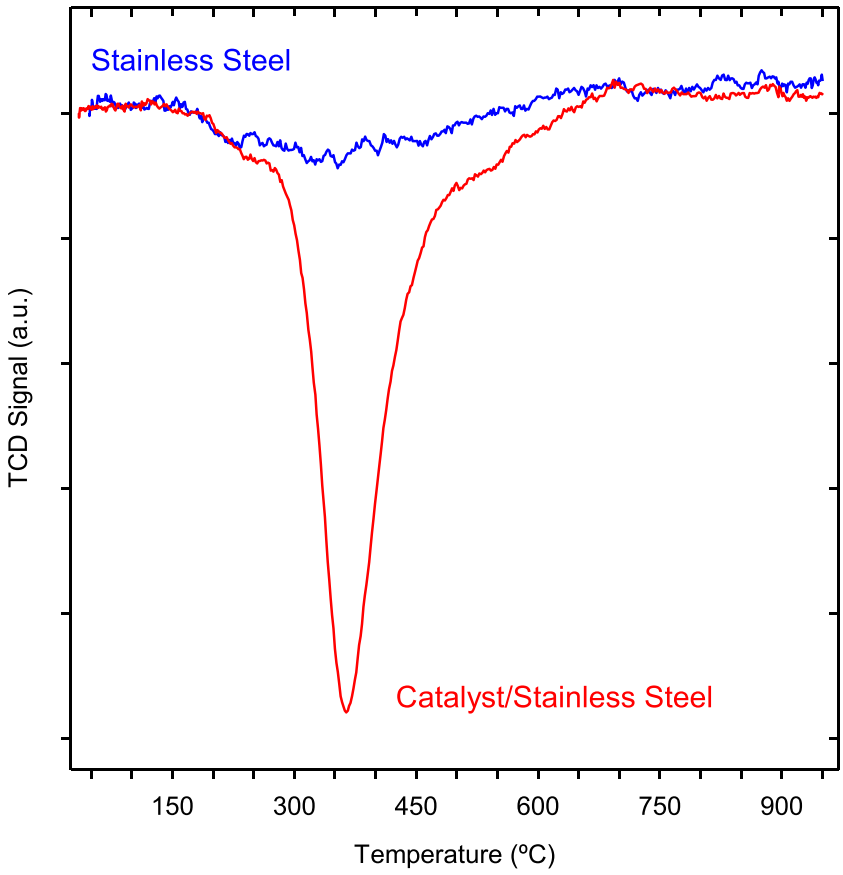

Fig. 4. H_2-TPR profiles of the bare and washcoated metallic monoliths under H_2(5%)Ar gas mixture and a heating rate of 10 °C min^{-1}.

performance at 900 °C.

Wang et al. [34] reported a maximum in the carbon production caused by CH_4 decomposition and/or the Boudouard reaction in the 557–700 °C range. From thermodynamic considerations, temperatures at around 900 °C were suggested as optima when a CO_2/CH_4 = 1:1 feed ratio is employed, since they allow a balance between the conversion achieved and the carbon accumulation [35]. Due to these precedents and the above commented results, we paid special attention to the catalytic behavior at 900 °C. Fig. 6 shows the reaction profiles versus time in the catalytic tests run at 900 °C with both washcoated and bare metallic monoliths. For comparison, the activity curves obtained in equivalent experiments using cordierite monoliths [14] are also included.

As can be seen, under the same experimental conditions, the washcoated metallic monolith exhibited an advantageous performance with respect to the corresponding washcoated cordierite. First, the conversion at the stationary state was higher, 95% and 75% for CO_2 and CH_4 respectively, and kept stable after 24 h of continuous operation. Second, in the case of the cordierite-supported Ni catalyst, a certain activation time was necessary at the beginning of the experiment, not observed for the metallic counterpart. This might be an indication of the positive influence of the honeycomb metallic nature on the heat transfer process. This effect and the stability behavior were also found operating at 750 and 800 °C (Figs. S3 and S4, respectively in ESI).

It is also interesting the comparison between the respective bare monoliths. While the bare cordierite as expected was almost completely inactive, the 3D-printed bare metallic monolith presented an activity at 900 °C far from negligible, with conversion values of 40% and 20% for CO_2 and CH_4, respectively (Fig. 6). This should be attributed to its inherent nickel content, which was evidenced by the characterization study. It also points to another advantage of the 3D printing metal honeycomb manufacture, the chance of selecting appropriate raw materials that may include already the active phase in the process to be applied, so avoiding or decreasing the need of external materials addition.

4. Conclusions

Honeycomb monolithic catalysts of nickel supported on CeO_2-ZrO_2 were prepared by the washcoating method, using metallic honeycomb

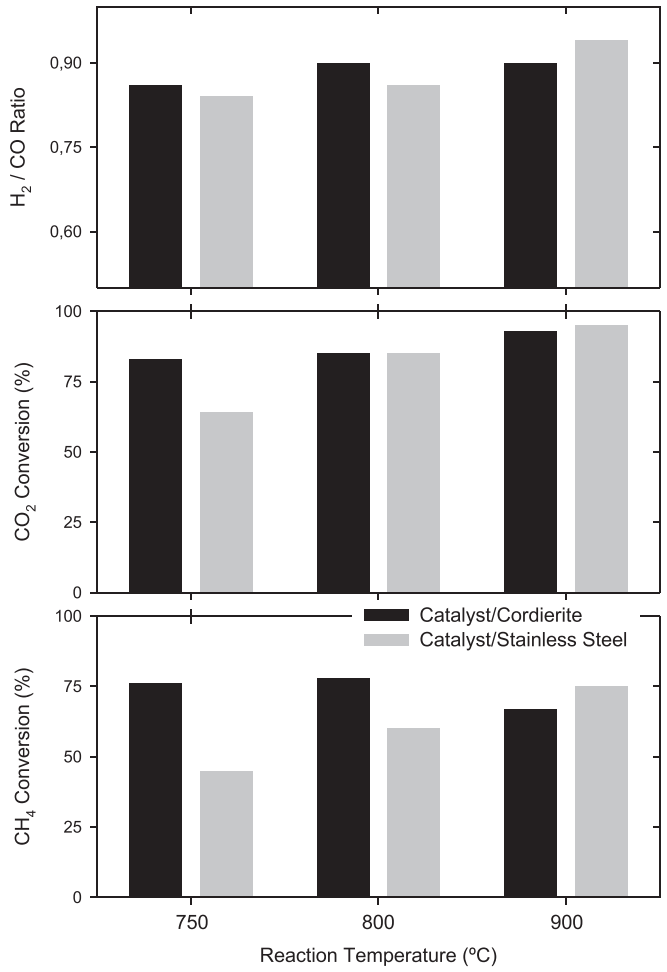

Fig. 5. Catalytic performance after 24 h in the DRM reaction of the washcoated metallic and cordierite monoliths. The cordierite-based samples used as reference were prepared according to a previous work [14].

monoliths as supports, the latter obtained by 3D printing from a commercial stainless-steel powder via direct laser sintering. The honeycombs had the same inner geometry (230 cpsi square cell section) and relatively well-adhered catalyst specific loading as those previously studied cordierite honeycombs washcoated by the same catalyst. They were tested also in the same reaction, dry reforming of methane (DRM), to facilitate the comparison and evaluate their potential. To the best of our knowledge, this was the first time that 3D-printing manufacture was employed to fabricate metal honeycombs with controlled geometry and applied to DRM, both aspects representing the major novelty of this research.

The 3D-printed monoliths did not only show an interesting performance as support of the nickel catalyst but also intrinsic activity by itself with reactants conversion values approaching 50% at 900 ˚C. This behavior was related to its initial nickel content as suggested by the characterization performed through XRF and SEM-EDX. Concerning the influence on the deposited nickel catalyst, the metal honeycomb allowed reaching almost full CO_2 conversion at 900 ˚C, not showing significant deactivation for long time of reaction, neither at this temperature nor at 800 or even at 750 ˚C. Moreover, it demonstrated an extra positive effect by eliminating the activation time in the DRM process previously observed over cordierite, which is a positive signal of heat transfer assistance.

The results obtained suggest that the approach proposed here might have great potential not only in the DRM but also in other catalytic processes by optimizing variables of the 3D printing methodology such as the raw material and geometry.

Declaration of Competing Interest

The authors declare no conflicts of interest.

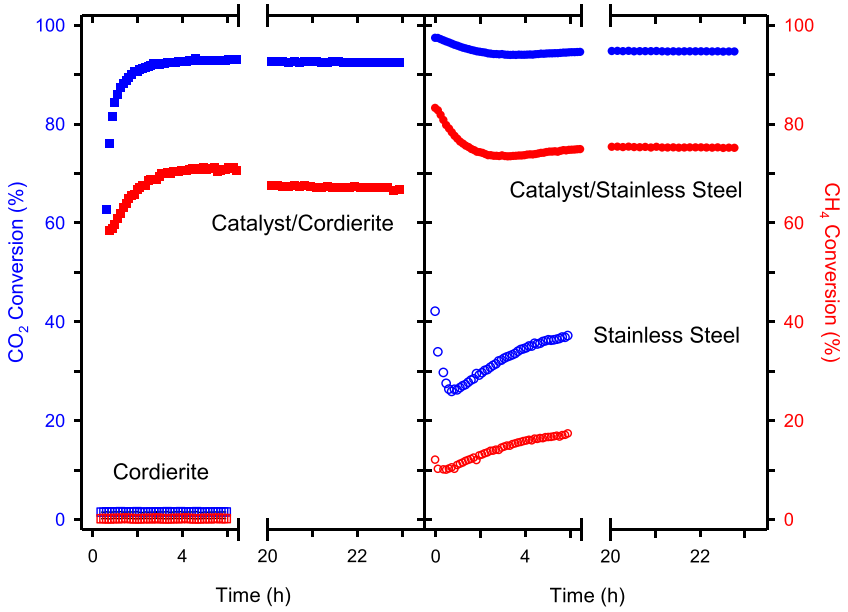

Fig. 6. Evolution with reaction time of the reactants conversion in the DRM reaction for the indicated samples operating at 900 ˚C with CH_4:CO_2 = 1:1 and WHSV = 115 L g^{-1} h^{-1}. The cordierite-based samples were prepared according to a previous work [14].

Acknowledgements

The authors thank the financial support by the Ministry of Economy and Competitiveness of Spain/FEDER Program of the EU (Project MAT2017-87579-R), and the Junta de Andalucía (Groups FQM-110 and FQM-334). We also acknowledge the Cadiz University SC-ICyT for using its facilities for the XRF and SEM-EDX measurements.

Appendix A. Supplementary data

Supplementary data to this article can be found online at https://doi.org/10.1016/j.catcom.2020.106181.

References

[1] R.M. Heck, S. Gulati, R.J. Farrauto, The application of monoliths for gas phase catalytic reactions, Chem. Eng. J. 82 (2001) 149–156, https://doi.org/10.1016/S1385-8947(00)00365-X.
[2] A. Montebelli, C.G. Visconti, G. Groppi, E. Tronconi, C. Christiani, C. Ferreira, S. Kohler, Methods for the catalytic activation of metallic structured substrates, Catal. Sci. Technol. 4 (2014) 2846–2870, https://doi.org/10.1039/c-4cy00179f.
[3] S. Govender, H.B. Friedrich, Monoliths: a review of the basics, preparation methods and their relevance to oxidation, Catalysts 7 (2017) 62, https://doi.org/10.3390/catal7020062.
[4] P. Avila, M. Montes, E.E. Miró, Monolithic reactors for environmental applications: a review on preparation technologies, Chem. Eng. J. 109 (2005) 11–36, https://doi.org/10.1016/j.cej.2005.02.025.
[5] F.J. Echave, O. Sanz, M. Montes, Washcoating of micro-channel reactors with PdZnO catalyst for methanol steam reforming, Appl. Catal. A 474 (2014) 159–167, https://doi.org/10.1016/j.apcata.2013.07.058.
[6] M.A. Peluso, L. Costa-Almeida, O. Sanz, J.E. Sambeth, H. Thomas, M. Montes, Washcoating of MnO_x on Fecralloy monoliths, Latin Amer. Appl. Res. 43 (2013) 301–306.
[7] M.R. Morales, B.P. Barbero, L.E. Cadús, MnCu catalyst deposited on metallic monoliths for total oxidation of volatile organic compounds, Catal. Lett. 141 (2011) 1598–1607, https://doi.org/10.1007/s10562-011-0687-y.
[8] C. Parra-Cabrera, C. Achille, S. Kuhn, R. Ameloot, 3D printing in chemical engineering and catalytic technology: structured catalysts, mixers and reactors, Chem. Soc. Rev. 47 (2018) 209–230, https://doi.org/10.1039/C7CS00631D.
[9] P. Michorczyk, E. Hędrzak, A. Węgrzyniak, Preparation of monolithic catalysts using 3D printed templates for oxidative coupling of methane, J. Mater. Chem. A 4 (2016) 18753, https://doi.org/10.1039/C6TA08629B.
[10] M. Kramer, M. McKelvie, M. Watson, Additive manufacturing of catalyst substrates for steam–methane reforming, J. Mater. Eng. Performance 27 (1) (2018) 21–31, https://doi.org/10.1007/s11665-017-2859-4.
[11] A. Quintanilla, J.A. Casas, P. Miranzo, M.I. Osendi, M. Belmonte, 3D-Printed Fe-doped silicon carbide monolithic catalysts for wet peroxide oxidation processes, Appl. Catal. B 235 (5) (2018) 246–255, https://doi.org/10.1016/j.apcatb.2018.04.066.
[12] C.R. Tubío, J. Azuaje, L. Escalante, A. Coelho, F. Guitián, E. Sotelo, A. Gil, 3D printing of a heterogeneous copper-based catalyst, J. Catal. 334 (2016) 110–115, https://doi.org/10.1016/j.jcat.2015.11.019.
[13] M. Lämmermann, G. Horak, W. Schwieger, H. Freund, Periodic open cellular structures (POCS) for intensification of multiphase reactors: liquid holdup and two-phase pressure drop, Chem. Eng. Process.: Process. Intensif. 126 (2018) 178–189, https://doi.org/10.1016/j.cep.2018.02.027.
[14] F. Agueniou, H. Vidal, M.P. Yeste, J.C. Hernández-Garrido, M.A. Cauqui, J.M. Rodríguez-Izquierdo, J.J. Calvino, J.M. Gatica, Ultrathin washcoat and very low loading monolithic catalyst with outstanding activity and stability in dry reforming of methane, Nanomaterials 10 (3) (2020) 445, https://doi.org/10.3390/nano10030445.
[15] P. Brussino, J.P. Bortolozzi, O. Sanz, M. Montes, M.A. Ulla, E.D. Banús, FeCrAlloy Monoliths Coated with Ni/Al2O3 Applied to the low-temperature production of ethylene, Catalysts 8 (2018) 291, https://doi.org/10.3390/catal8070291.
[16] S. Allahyari, M. Haghighi, A. Ebadi, Direct conversion of syngas to DME as a green fuel in a high pressure microreactor: influence of slurry solid content on characteristics and reactivity of washcoated CuO–ZnO–Al_2O_3/HZSM-5 nanocatalyst, Chem. Eng. Process. 86 (2014) 53–63, https://doi.org/10.1016/j.cep.2014.10.001.
[17] F. Meng, G. Chen, Y. Wanga, Y. Liu, Metallic Ni monolith–Ni/$MgAl_2O_4$ dual bed catalysts for the autothermal partial oxidation of methane to synthesis gas, Int. J. Hydrog. Energy 35 (2010) 8182–8190, https://doi.org/10.1016/j.ijhydene.2009.12.144.
[18] N. de Miguel, J. Manzanedo, J. Thormann, P. Pfeifer, P.L. Arias, Ni catalyst coating on Fecralloy® Microchanneled foils and testing for methane steam reforming, Chem. Eng. Technol. 33 (1) (2010) 155–166, https://doi.org/10.1002/ceat.200900439.
[19] S. Katheria, G. Deo, D. Kunzru, Washcoating of Ni/$MgAl_2O_4$ catalyst on FeCralloy monoliths for steam reforming of methane, Energy Fuel 31 (2017) 3143–3153, https://doi.org/10.1021/acs.energyfuels.6b03423.
[20] T. Hirano, Y. Xu, Catalytic properties of a pure Ni coil catalyst for methane steam reforming, Int. J. Hydrog. Energy 42 (2017) 30621–30629, https://doi.org/10.1016/j.ijhydene.2017.10.135.
[21] M.A. Ashraf, O. Sanz, M. Montes, S. Specchia, Insights into the effect of catalyst loading on methane steam reforming and controlling regime for metallic catalytic monoliths, Int. J. Hydrog. Energy 43 (2018) 11778–11792, https://doi.org/10.1016/j.ijhydene.2018.04.126.
[22] J.M. Gatica, J.C. Hernández-Garrido, H. Vidal, Porosity enhancement in non-cordierite honeycomb monoliths, Adv. Mater. Sci. Res. 38 (2019) 147–189.
[23] D.M. Gómez, J.M. Gatica, J.C. Hernández-Garrido, G.A. Cifredo, M. Montes, O. Sanz, J.M. Rebled, H. Vidal, A novel CoO_x/La-modified-CeO_2 formulation onto cordierite honeycomb catalysts with application in VOCs oxidation, Appl. Catal. B 144 (2014) 425–434, https://doi.org/10.1016/j.apcatb.2013.07.045.
[24] S.A. Adegbite, Coating of Catalyst Supports: Links Between Slurry Characteristics, Coating Process and Final Coating Quality, University of Birmingham Doctoral Thesis (2010).
[25] S. Zhaoa, J. Zhanga, D. Wenga, X. Wua, A method to form well-adhered γ-Al_2O_3 layers on FeCrAl metallic supports, Surf. Coat. Technol. 167 (2003) 97–105, https://doi.org/10.1016/S0257-8972(02)00859-9.
[26] J. Jia, J. Zhou, J. Zhang, Z. Yuan, S. Wang, The influence of preparative parameters on the adhesion of alumina washcoats deposited on metallic supports, Appl. Surf. Sci. 253 (2007) 9099–9104, https://doi.org/10.1016/j.apsusc.2007.05.034.
[27] A. Kambolis, H. Matralis, A. Trovarelli, Ch. Papadopoulou, Ni/CeO_2-ZrO_2 catalysts for the dry reforming of methane, Appl. Catal. A 377 (2010) 16–26, https://doi.org/10.1016/j.apcata.2010.01.013.
[28] H.-S. Roh, H.S. Potdar, K.-W. Jun, J.-W. Kim, Y.-S. Oh, Carbon dioxide reforming of methane over Ni incorporated into Ce–ZrO_2 catalysts, Appl. Catal. A 276 (2004) 231–239, https://doi.org/10.1016/j.apcata.2004.08.009.
[29] J.A. Montoya, E. Romero-Pascual, C. Gimon, P. Del Angel, A. Monzon, Methane reforming with CO_2 over Ni/ZrO_2–CeO_2 catalysts prepared by sol–gel, Catal. Today 63 (2000) 71–85, https://doi.org/10.1016/S0920-5861(00)00447-8.
[30] J. Chen, Q. Wu, J. Zhang, J. Zhang, Effect of preparation methods on structure and performance of Ni/$Ce_{0.75}Zr_{0.25}O_2$ catalysts for CH_4–CO_2 reforming, Fuel 87 (2008) 2901–2907, https://doi.org/10.1016/j.fuel.2008.04.015.
[31] M.A. Muñoz, J.J. Calvino, J.M. Rodríguez-Izquierdo, G. Blanco, D.C. Arias, J.A. Pérez-Omil, J.C. Hernández-Garrido, J.M. González-Leal, M.A. Cauqui, M.P. Yeste, Highly stable ceria-zirconia-yttria supported Ni catalysts for syngas production by CO_2 reforming of methane, Appl. Surf. Sci. 426 (2017) 864–873, https://doi.org/10.1016/j.apsusc.2017.07.210.
[32] Y. Wang, L. Yao, S. Wang, D. Mao, C. Hu, Low-temperature catalytic CO_2 dry reforming of methane on Ni-based catalysts: a review, Fuel Process. Technol. 169 (2018) 199–206, https://doi.org/10.1016/j.fuproc.2017.10.007.
[33] W.-J. Jang, D.-W. Jeong, J.-O. Shim, H.-M. Kim, H.-S. Roh, I.H. Son, S.J. Lee, Combined steam and carbon dioxide reforming of methane and side reactions: thermodynamic equilibrium analysis and experimental application, Appl. Energy 173 (2016) 80–91, https://doi.org/10.1016/j.apenergy.2016.04.006.
[34] S. Wang, G.Q. Lu, G.J. Millar, Carbon dioxide reforming of methane to produce synthesis gas over metal-supported catalysts: state of the art, Energy Fuel 10 (1996) 896–904, https://doi.org/10.1021/ef950227t.
[35] W.-J. Jang, J.-O. Shim, H.-M. Kim, S.-Y. Yoo, H.-S. Roh, A review on dry reforming of methane in aspect of catalytic properties, Catal. Today 324 (2019) 15–26, https://doi.org/10.1016/j.cattod.2018.07.032.